



Hot Corrosion Performance of Plasma-Sprayed Multiwalled Carbon Nanotube–Al₂O₃ Composite Coatings in a Coal-Fired Boiler at 900 °C

Rakesh Goyal, Buta Singh Sidhu, and Vikas Chawla

(Submitted August 25, 2019; in revised form July 25, 2020; published online September 2, 2020)

The present study investigates the high-temperature corrosion behavior of plasma-coated boiler steel for 1000 h in a 110-MW water tube boiler, which had encountered severe corrosion and the tube failure. The coating was carried out by alumina and MWCNTs (multiwalled carbon nanotubes)-reinforced alumina composite powders. The uncoated and coated steel substrates were hung at a platen superheater at 900 °C. After the exposure, thermogravimetric analysis was carried out to evaluate the kinetics of corrosion. XRD, SEM, TEM and EDS analysis was carried out to evaluate the corrosion products at the end of the cyclic high-temperature corrosion. The present research work concludes that CNT-reinforced alumina coatings (4.0 wt.% CNT + Al₂O₃ coating) have decreased the corrosion rate to 30.72 mpy, which was 113.53 mpy for conventional alumina coatings and 376.96 mpy for bare T11 boiler steel in the boiler environment. This manuscript submits the failure of tube at the platen superheater, exposure conditions and the analysis of the coated and uncoated samples of the steel tubes.

Keywords carbon nanotubes, ceramics matrix, corrosion and wear, composites, plasma spraying, steel, x-ray

1. Introduction

Hot corrosion mostly occurs in the components of turbines, boilers and waste incinerators due to very high temperatures (Ref 1, 2). The increase in operating temperatures over the years has also led to an increase in the problem of hot corrosion in these industrial components. In the recent past, the use of low-grade fuels has been increased, and this has led to requirement of specific attention to hot corrosion (Ref 3-5). Many types of impurities such as S, Na, V and K are present in the low-grade fuels, and these impurities melt at low temperatures and form compounds such as Na₂SO₄, V₂O₅ and vanadates which get deposited on the components and start corrosion (Ref 6-8). At high temperatures, these deposited compounds destroy the oxide layers on the top of materials and thereby accelerate the corrosion rate (Ref 2).

In the recent past, some authors have used thermal spray coatings to improve the corrosion resistance of these compo-

nents (Ref 49-53). Among these thermal spray techniques, the plasma spraying is an important versatile technique which was utilized to spray coatings of metals, ceramic materials and their mixtures on the boiler components (Ref 7, 9-11). Plasma spraying technique has been used successfully to deposit alumina (Al₂O₃), calcia-stabilized zirconia and other similar materials (Ref 9, 12-14). Alumina is a ceramic material and has high hardness and chemical inertness, and it retains its properties even at 1100 °C (Ref 15). The literature reveals that alumina is having high corrosion resistance than other materials (Ref 16, 17). The coating consists of cracks and voids at their splat boundaries, and these cracks give passage to corrosive agents to pass through these and induce corrosion (Ref 18-20). Thus, corrosion resistance may be increased by decreasing the extent of these voids and cracks (Ref 21).

CNTs are nanofibers which were invented in 1991. CNTs have very exceptional mechanical and electrical properties. These are hundreds of times stronger than carbon steels with a high value of modulus (Ref 22-25). These are therefore suitable reinforcement material for the composites (Ref 21, 26, 27). In the recent past, a few researchers have developed composite coatings with CNTs as reinforcements (Ref 28, 29). A few researchers had studied the wear behavior of CNTs–Al₂O₃ composite coatings (Ref 30-34).

It is revealed from the above discussion that thermal spray coatings can enhance the corrosion resistance of boiler steels at high temperature. There is a very limited research available in the case of CNT-reinforced composite coatings for various industrial applications. So, there is still a big scope to investigate hot corrosion behavior of CNTs–alumina mix composite coatings on boiler steels in actual boiler. The aim of this investigation is to research the high-temperature corrosion behavior of plasma-sprayed alumina and CNTs–Al₂O₃ composite coatings (with different percentages of CNTs) on T11 boiler tube steel in actual boiler environment. The resulting corrosion products were analyzed by SEM, EDS, TEM and XRD analysis.

Rakesh Goyal, Chitkara University Institute of Engineering & Technology, Chitkara University, Punjab, India; **Buta Singh Sidhu**, Department of Mechanical Engineering, MRS Punjab Technical University, Bathinda, Punjab, India; and **Vikas Chawla**, Department of Mechanical Engineering, IKG Punjab Technical University, Kapurthala, Punjab, India. Contact e-mail: rakesh.goyal@chitkara.edu.in.

2. Experimental Details

2.1 Substrate Material, Development and Characterization of Coatings

ASME-SA213-T11 boiler steel used in this investigation was procured in the tube form from Guru Nanak Dev Thermal Power Plant, Bathinda, Punjab. The specimens with $20 \times 15 \times 5$ mm dimensions were made from the tube. These specimens were polished using SiC emery papers of 220, 400 and 600 grit sizes and subsequently on 1/0, 2/0, 3/0 and 4/0 grades. The actual and nominal chemical composition of the substrate steel was examined at the CITCO-IDFC Testing Laboratory, Chandigarh, and the result is given in Table 1.

Four different composite coatings were prepared by blending Al_2O_3 (powder size $40 \pm 10 \mu\text{m}$; minimum assay 99%, Spraymet, Karnataka, India) with 0, 1.5, 2 and 4 wt.% CNTs (multiwalled; powder size is outer diameter \times L = $6\text{-}9 \text{ nm} \times 5 \mu\text{m}$; minimum assay 95%, Sigma-Aldrich Chemicals, USA) in a laboratory ball mill, using a low-energy ball milling method. The mixtures were rolled for 4 h continuously with a speed of 200 rpm (Ref 35). All the six faces of the substrate were coated. Firstly, Ni-Cr powder (Powder Alloy Coppn, Ohio, USA) has been deposited as a bond coat, and then, the coatings were deposited on the substrates at Anod Plasma Ltd., Kanpur, India, by using 40 kW Miller Thermal (USA) plasma spray apparatus. The coating powders used and their compositions were: $0\text{CAI}_2\text{O}_3$ (Al_2O_3 -0 wt.% CNT), $1.5\text{CAI}_2\text{O}_3$ (Al_2O_3 -1.5 wt.% CNT), $2\text{CAI}_2\text{O}_3$ (Al_2O_3 -2 wt.% CNT) and $4\text{CAI}_2\text{O}_3$ (Al_2O_3 -4 wt.% CNT). All the process parameters were tested and optimized before spraying. The deposition parameters are summarized in Table 2.

The as-coated samples were submitted to metallography, SEM, EDS, XRD and x-ray mapping analysis. The literature related to deposition and characterization of these coatings has been published elsewhere by the same authors (Ref 35). The coating thickness was measured from the backscattered electron (BSE) cross-sectional images and was in the range of $200 \pm 10 \mu\text{m}$. A 'LEICA Image analyzer' (Germany made) was used to check the porosity values. As the percentage of CNTs in the coating composition increases, the porosity of CNT- Al_2O_3 coatings was observed decreasing. The porosity of Al_2O_3 -coated specimen was determined to be higher than 4%, and the porosity was found to be less than 4%, with the addition of CNTs in Al_2O_3 powder. The tensile adhesion test (TAT) specified by ASTM C-633 was used to measure the adhesion strength of the coating. To reveal the adhesive strength of coatings, mild steel was used as a substrate (length and diameter—25.4 mm both). Alumina grits were used for grit blasting the substrates. Then, spray coating was applied onto the flat end of cylindrical specimens. HTK Ultrabond 100 adhesive was applied between two coated flat ends of the cylindrical specimens. After 80 min of curing at 150°C in an oven at ambient atmosphere, the bonded rods were naturally

cooled to room temperature. The coating pullout test was carried out using the H50K-S UTM Benchtop Materials Tester supplied by Tinius Olsen, England, at a crosshead speed of 1 mm/min at IIT Ropar. The moment the coating got torn off from the specimen, the reading (of the load), which corresponds to the bond strength of coating, was recorded (Ref 35, 54). The adhesion strength of the CNTs-mixed coatings was also increased with the enhancement in CNTs content. The adhesion strength was measured as 17.6 MPa for $4\text{CAI}_2\text{O}_3$ coatings, whereas that for $0\text{CAI}_2\text{O}_3$ was 11.7 MPa. The CNTs were noticed to be uniformly dispersed in the alumina alloy powder after mixing as shown in Fig. 1(a) and (b) in the TEM analysis. And CNTs were observed to be uniformly present in the Al_2O_3 matrix in $4\text{CAI}_2\text{O}_3$ -coated steel as shown in FE-SEM and EDS analysis in Fig. 2. CNTs have been chemically stable during the spray process. There was not any formation of carbides as well as oxides regardless of the high temperature.

2.2 Hot Corrosion Studies in Actual Boiler Environment

Hot corrosion examination was executed for the uncoated as well as coated substrates in actual boiler environment for ten cycles, at GNDTPP, Bathinda, Punjab, India. One cycle consisted of 100 h of heating on boiler at 900°C with a fluctuation of $\pm 10^\circ\text{C}$ and 1 h of cooling in still air. The samples were hung 31 m high from the boiler base by a stainless steel wire. The degradation behavior was appraised using cumulative weight gain data, metal thickness loss and depth of corrosion attack. XRD, SEM, EDS and x-ray mapping techniques were applied to examine the corroded steel samples.

3. Results

3.1 Visual Examination

After every cycle, each specimen was visually examined for variation in color, luster and development of cracks in the oxide scale. After the completion of ten cycles, the specimens were finally examined and their macrographs were taken. The macrographs for uncoated and coated specimens after exposure

Table 2 The process parameters during plasma spray process

Plasma spray parameters	Bond coat	Alumina
Arc current, A/voltage, V	550/50	550/50
Argon pressure, psi	60	60
Hydrogen pressure, psi	10	10
Spraying distance, mm	90-110	90-110
Hopper RPM	6.5	1.5
Powder gas pressure, psi	50	45

Table 1 Chemical composition (wt.%) of grade T11 boiler steel

ASME code	Composition	C	Mn	Si	S	P	Cr	Mo	V	Ni	Fe
SA213-T-11	Nominal	0.15	0.3-0.6	0.5-1	0.03	0.03	1-1.5	0.44-0.65	—	—	Bal.
	Actual	0.1911	0.6281	0.3380	0.0128	0.0136	1.064	0.01	0.0217	0.517	Bal.

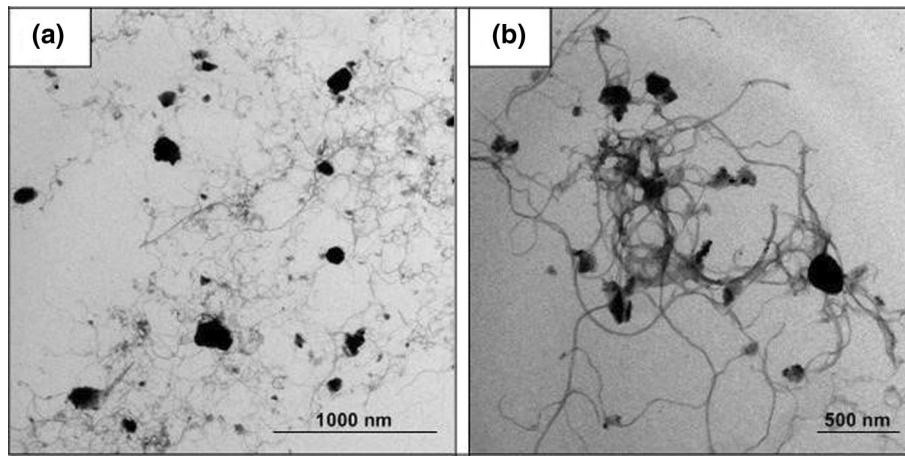


Fig. 1 (a-b) TEM images showing dispersed CNTs in alumina alloy powder in $4\text{CAI}_2\text{O}_3$.

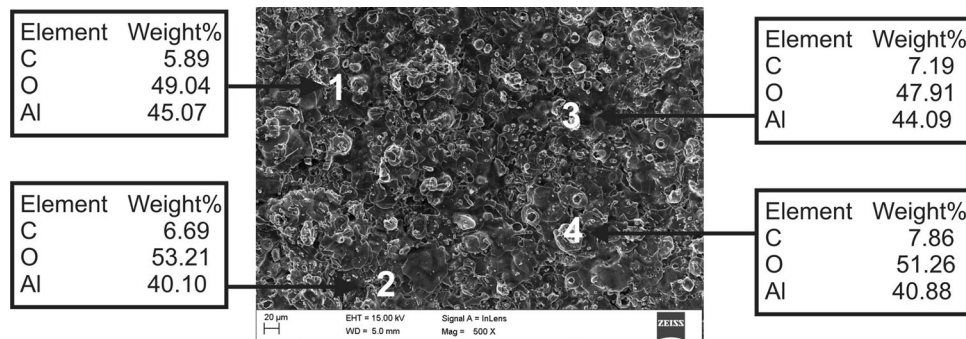


Fig. 2 FE-SEM and EDS analysis for $4\text{CAI}_2\text{O}_3$ -coated T11 steel.

to boiler environment at $900\text{ }^\circ\text{C}$ for 1000 h are shown in Fig. 3(a), (b), (c), (d) and (e).

For the uncoated boiler steel substrate, from the first cycle onward, a scale appeared on the surface, which is dark black gray in color. Ash has been deposited on the sample just after the completion of the first cycle. The sample showed spalling when it is exposed in the boiler environment. Severe spalling and ash deposition of the bare T11 steel were continued until the last cycle. The ash has been removed from the sample by washing it with acetone. The weight of the specimens was recorded after the completion of each cycle. After the completion of the 1000-h cyclic study, ash deposited with fragile scale indicating severe spalling and dark gray-colored surface appearance on the surface and brownish-colored scale in the middle was observed (Fig. 3a). For the alumina-coated T11 boiler steel, blackish gray-colored oxide scale was seen at the last of the study. Top scale spalling was also detected at some brownish-colored areas, as shown in Fig. 3(b). Ash deposition was seen just after the first cycle and until the end. Macrographs of CNT- Al_2O_3 -coated T11 steels after exposure of 1000 h at about $900\text{ }^\circ\text{C}$ are shown in Fig. 3(c), (d) and (e). For all the CNT- Al_2O_3 -coated steels, the color of scale was noticed to be brown after the first cycle of 100 h. After that, the fading of brown color has been initiated but it remained until the end of the cyclic study. No spalling was observed, and the scale was intact even after 1000 h of exposure. The dark gray patches on the scale may be due to ash deposition.

3.2 Weight Change and Thickness Loss data

Figure 4 indicates the cumulative weight gain/unit area (mg/cm^2) for all the specimens after for 1000-h cyclic examination. The net weight gain represents the resulting effect of weight gain due to oxide-scale formation and weight loss because of spalling of scale. The overall weight gain by the bare steel has come out to be $135.96\text{ mg}/\text{cm}^2$. This higher weight gain, for uncoated steel as compared to coated steels, has been due to the formation of thick oxide scale. The weight gain of conventional Al_2O_3 -coated T11 steel has been found to be $113.27\text{ mg}/\text{cm}^2$. The overall weight gain of $1.5\text{CAI}_2\text{O}_3$ -coated, $2\text{CAI}_2\text{O}_3$ -coated and $4\text{CAI}_2\text{O}_3$ -coated T11 steel was determined to be 68.59, 33.82 and $11.27\text{ mg}/\text{cm}^2$, respectively. It shows that with the addition of CNTs content in the Al_2O_3 , the weight gain of coated steel decreases. $4\text{CAI}_2\text{O}_3$ -coated T11 steel exhibited minimum overall weight gain among all types of coatings.

The weight gain data could not be used for forecasting corrosion behavior owing to spalling and ash deposition on specimens. Although ash has been washed off with acetone, it is not possible to remove the ash completely. Therefore, the extent of corrosion of these exposed specimens was studied with the help of thickness loss of each specimen. The 'mpy' is the rate of corrosion in mils per year and indicates the depth of corrosion in mils for a complete-year exposure. One mil is 1000th part of an inch. In the present research, the exposure time is 1000 h and the penetration of corrosion is measured in mm, which was converted into mpy to mention the corrosion rate (Ref 52).

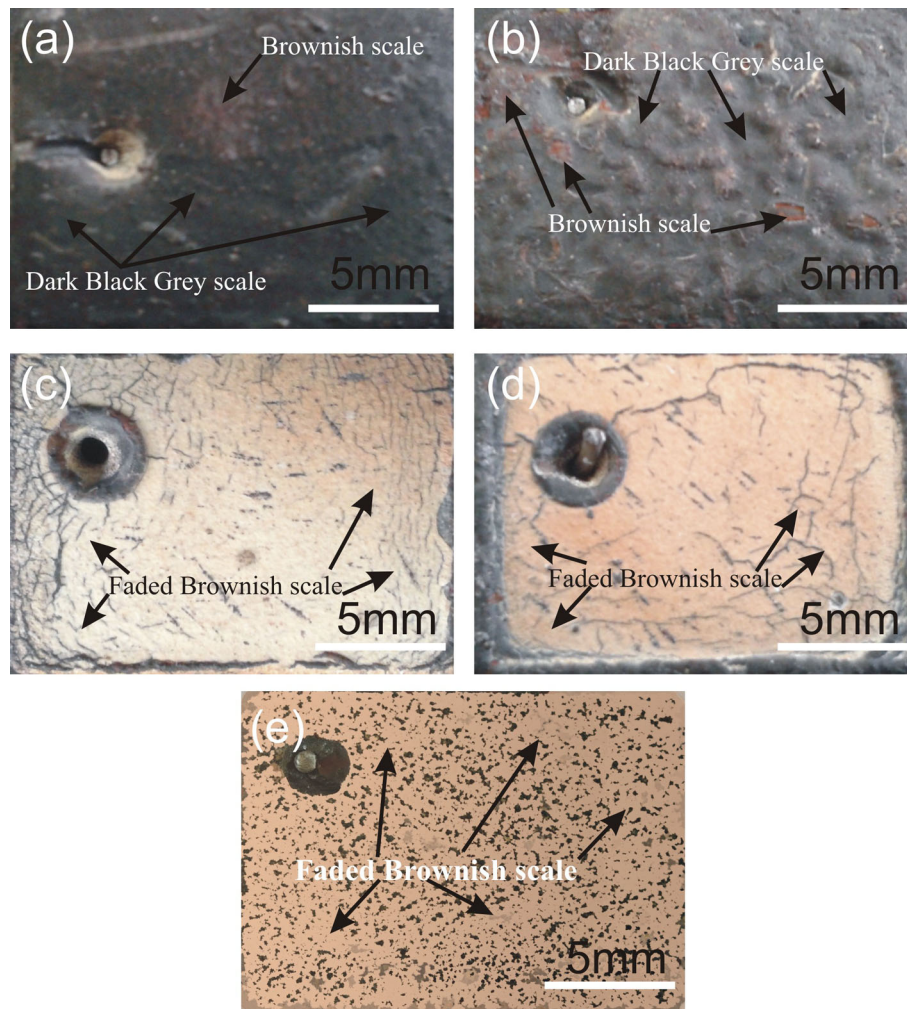


Fig. 3 Macrographs of (a) bare T11 steel, (b) $0\text{Al}_2\text{O}_3$ coating, (c) $1.5\text{Al}_2\text{O}_3$ coating, (d) $2\text{Al}_2\text{O}_3$ coating, (e) $4\text{Al}_2\text{O}_3$ coating after exposure to thermal environment.

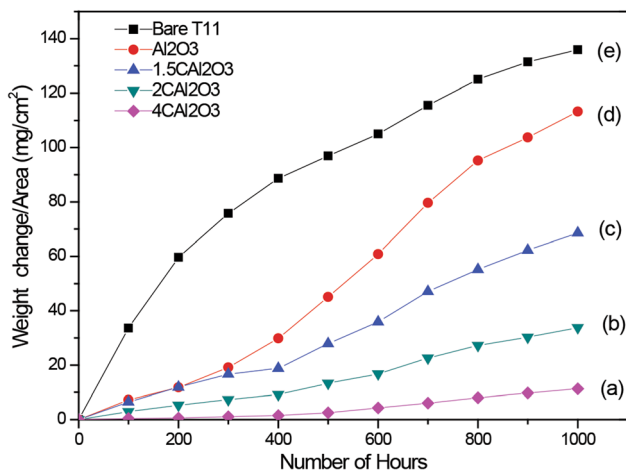


Fig. 4 Cumulative weight gain per unit area for (a) bare T11 steel, (b) $0\text{Al}_2\text{O}_3$ coating, (c) $1.5\text{Al}_2\text{O}_3$ coating, (d) $2\text{Al}_2\text{O}_3$ coating, (e) $4\text{Al}_2\text{O}_3$ coating.

The loss of thickness of the bare steel after exposure has been measured as 1.093 mm as observed in cross-sectional view. Thus, corrosion rate comes out to be 376.96 mpy

after conversion in mils/year (mpy). Further, on the basis of thickness loss data recorded, the corrosion rates of the coatings were measured as 113.53, 43.63, 36.51 and 30.72 mpy for $0\text{Al}_2\text{O}_3$ -coated, $1.5\text{Al}_2\text{O}_3$ -coated, $2\text{Al}_2\text{O}_3$ -coated and $4\text{Al}_2\text{O}_3$ -coated steel, respectively, and are shown in Fig. 5.

3.3 X-ray Diffraction Analysis

X-ray peaks for the uncoated, $0\text{Al}_2\text{O}_3$ -, $1.5\text{Al}_2\text{O}_3$ -, $2\text{Al}_2\text{O}_3$ - and $4\text{Al}_2\text{O}_3$ -coated steels after exposure are shown in Fig. 6(a), (b), (c), (d) and (e), respectively. The formation of oxides of Fe could be identified in the case of uncoated steel. The prominent phase noticed for this steel is Fe_2O_3 (JCPDS No. 00-002-1047) and SiO_2 (JCPDS No. 00-001-0649) and Cr_2O_3 (JCPDS No. 00-001-1294) as minor phase (Fig. 6a). Al_2O_3 -coated T11 steel uncovered to the boiler surroundings has indicated the formation of Al_2O_3 (JCPDS No. 10-173) as the main phase along with Na_2O (JCPDS No. 00-003-1074), SiO_2 , NiO (JCPDS No. 00-022-1189) and Cr_2O_3 (Fig. 6b). In the cases of $1.5\text{Al}_2\text{O}_3$ -, $2\text{Al}_2\text{O}_3$ - and $4\text{Al}_2\text{O}_3$ -coated T11 steels (Fig. 6c, d and e), Al_2O_3 was the major phase and C (JCPDS No. 00-0010640), Na_2O and SiO_2 have been observed as the minor XRD phases.

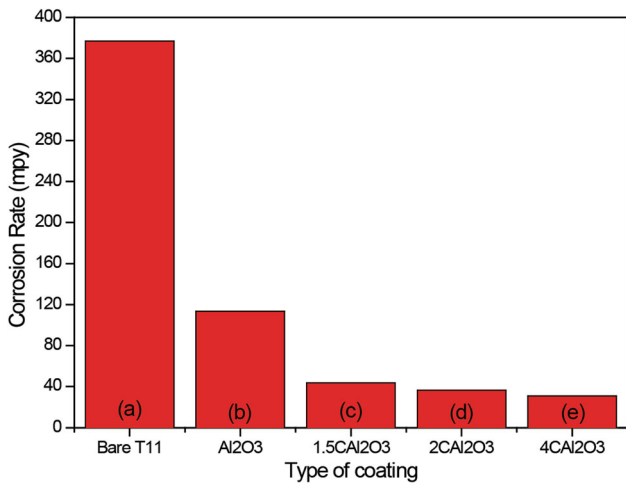


Fig. 5 Corrosion rate in mils per year (mpy) for (a) Bare T11 steel, (b) 0Al₂O₃ coating, (c) 1.5Al₂O₃ coating, (d) 2Al₂O₃ coating, (e) 4Al₂O₃ coating.

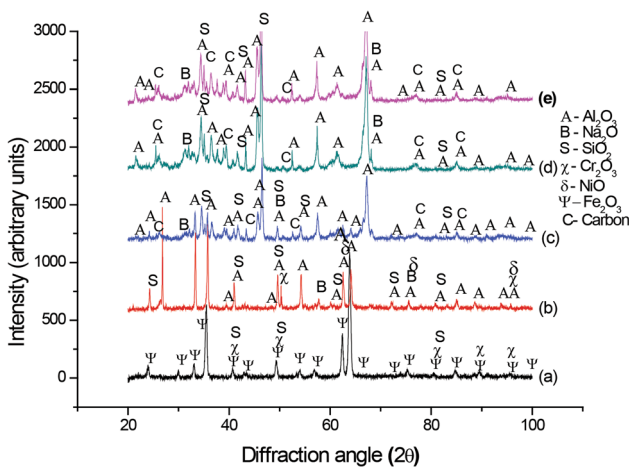


Fig. 6 XRD pattern for the (a) bare, (b) 0Al₂O₃-coated, (c) 1.5Al₂O₃-coated, (d) 1.5Al₂O₃-coated, (e) 4Al₂O₃-coated T11 steel after exposure.

3.4 FE-SEM and EDS Analysis

FE-SEM and EDS analysis for uncoated and plasma spray-coated T11 samples after exposure is presented in Fig. 7. The surface morphology of bare T11 steel indicated the granular scale as presented in Fig. 7(a). The micrograph indicates the scale developed with blackish gray and white regions. Also the surface shows the signs of erosion. Excessive corrosion could be experienced on the surface of specimen. The EDS analysis of uncoated T11 steel substrates at points 1 and 2 in the micrograph shows the presence of Si, Al and O along with Fe. This may be because of the ash contents present on the specimen. This clearly indicates the formation of Fe₂O₃ mainly and some amounts of SiO₂. The micrograph of the Al₂O₃-coated corroded specimen (Fig. 7b) points the presence of mainly Al, Ni, Cr, Si and O element at points 1 and 2, which may be oxide layer of alumina and ash. The scale consists of white and dark gray regions.

The micrograph of 1.5Al₂O₃-coated T11 steel (Fig. 7c) indicates a higher amount of O than Al in the composition and

minor percentage of C is also visible in the scale, at both the points. The EDS analysis for the scale of 2Al₂O₃-coated T11 steel indicated in Fig. 7(d) shows the presence of Al, O and C. The FE-SEM micrograph of 4Al₂O₃-coated T11 steel is shown in Fig. 7(e). The presence of O, Al and C can be clearly seen in the scale after hot corrosion in actual boiler environment. Ash particles such as Al, Si, V and Ca can also be seen imbedded in scale as white color nodules.

3.5 Cross-sectional Analysis of the Scale

SEM micrographs and elemental variation throughout the cross section of coated as well as uncoated T11 steel revealed to the coal-fired boiler surroundings at 900 °C for 1000 h are presented in Fig. 8(a), (b), (c), (d) and (e). SEM micrograph of the uncoated T11 steel in Fig. 8(a) indicates thick scale. The scale has cracks and dark spots and is fragile with the significant amount of corrosion. The oxygen is present in the significant amount throughout the scale. Therefore, there seems a tendency of Fe₂O₃ in the oxide scale.

The micrographs shown in Fig. 8(b) for the revealed cross section of Al₂O₃-coated T11 steel indicate continuous adherent scale. The scale has cracks at many locations. The scale comprises Al, O and Si clearly showing the presence of oxides of aluminum and ash for conventional alumina coating. The voids can be seen in coating scale. Ni and Cr elements at point 2 can also be seen. The micrograph for the cross section of 1.5Al₂O₃ coating is shown in Fig. 8(c). In scale, C is observed in major proportion (points 3 to 6), pointing the presence of CNTs in the coating matrix. The micrographs for 2Al₂O₃- and 4Al₂O₃-coated T11 steel after exposure are shown in Fig. 8(d), (e) and (f). The significant amount of C is present in the scale (points 3 to 6) due to the presence of CNTs in the alumina coating. Coating layer is intact.

3.6 X-ray Mapping Analysis

X-ray mappings for a section of oxide scale of uncoated as well as coated specimens are presented in Fig. 9-11. The micrograph of bare T11 steel (Fig. 9) depicts significant corrosion along scale-substrate interface and the formation of dense oxide scale. Mainly, the scale of iron oxide has been composed. The O has been seen penetrating deep into the substrate, as pointed by x-ray mapping.

The x-ray mapping for Al₂O₃-coated T11 boiler steel points the presence of Al, Fe and O throughout the scale along with Ni and Cr near the interface (Fig. 10). For 1.5Al₂O₃-coated T11 boiler steel, the BSEI and x-ray mappings are shown in Fig. 11. The x-ray mapping indicates the presence of Al and O along with minor traces of C throughout the scale. Similar x-ray mapping results were observed for 2Al₂O₃- and 4Al₂O₃-coated T11 boiler steel. But, the traces of C become more significant, with the increase of CNTs (from 1.5 to 4%) in the composite coating. The x-ray mappings indicate that the interface between coating and substrate is plentiful in Ni and Cr. This evinces the presence of bond coat at the interface.

4. Discussion

Fragile scale with tendency to spall was noticed for the bare T11 steel. The ash deposition, erosion and tendency to spall were continued during the experimentation. Also, the higher

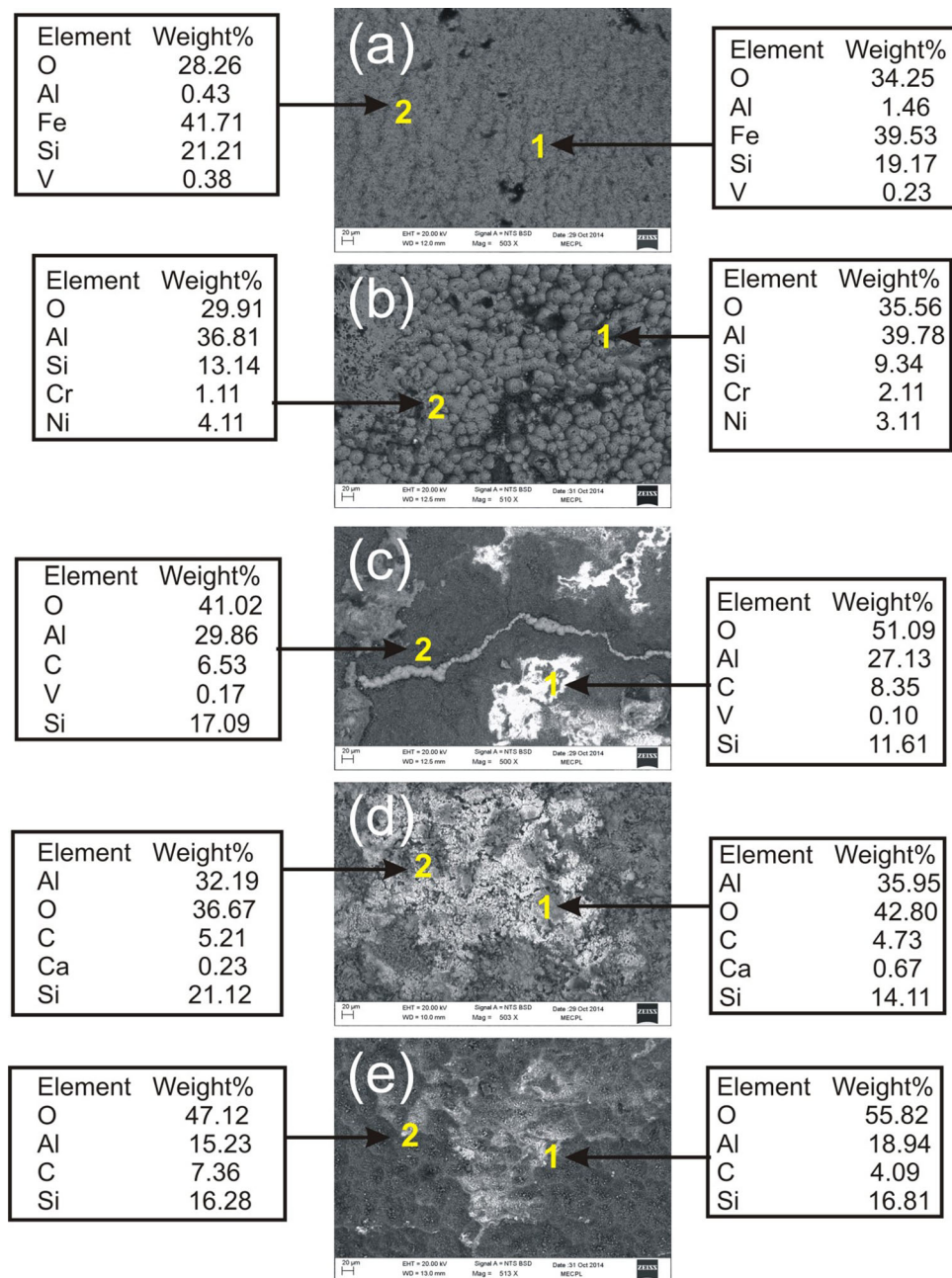


Fig. 7 FE-SEM and EDS analysis for (a) bare T11 steel, (b) 0CaAl₂O₃ coating, (c) 1.5CaAl₂O₃ coating, (d) 2CaAl₂O₃ coating, (e) 4CaAl₂O₃ coating after exposure to boiler.

corrosion rate of bare T11 steel was due to spalling and fluxing of oxide scale during exposure.

The coal used in GNDTPP, Bathinda, is having 34.52% ash content. Further, this ash contains Na₂O (0.34%) and K₂O (1.35%) and interacts with the flue gases of the boiler (SO₂, SO₃, O₂, etc.). Weulersse-Mouturat et al. (Ref 36) reported that ash content is generated due to burning of coal. The settlement of these low-melting-point elements initiates hot corrosion on the surface of boiler tubes (Ref 37). The most widely

recognized deposit detected on boiler tubes is sodium vanadyl vanadate having low melting point, and it corrodes steel by long-term contact (Ref 38). The interaction of ash with gas in boiler leads to the deposition of alkali sulfates (K₂SO₄, Na₂SO₄) and reacts with iron oxides in the presence of SO₃ to form alkali-ion trisulfates (Na, K)₃Fe(SO₄)₃. These compounds are in molten state at boiler temperature: 624 °C for Na₃Fe(SO₄)₃, 618 °C for K₃Fe(SO₄)₃ and 552 °C, for the mixed compound (Na, K)₃Fe(SO₄)₃ (Ref 39, 40). These react

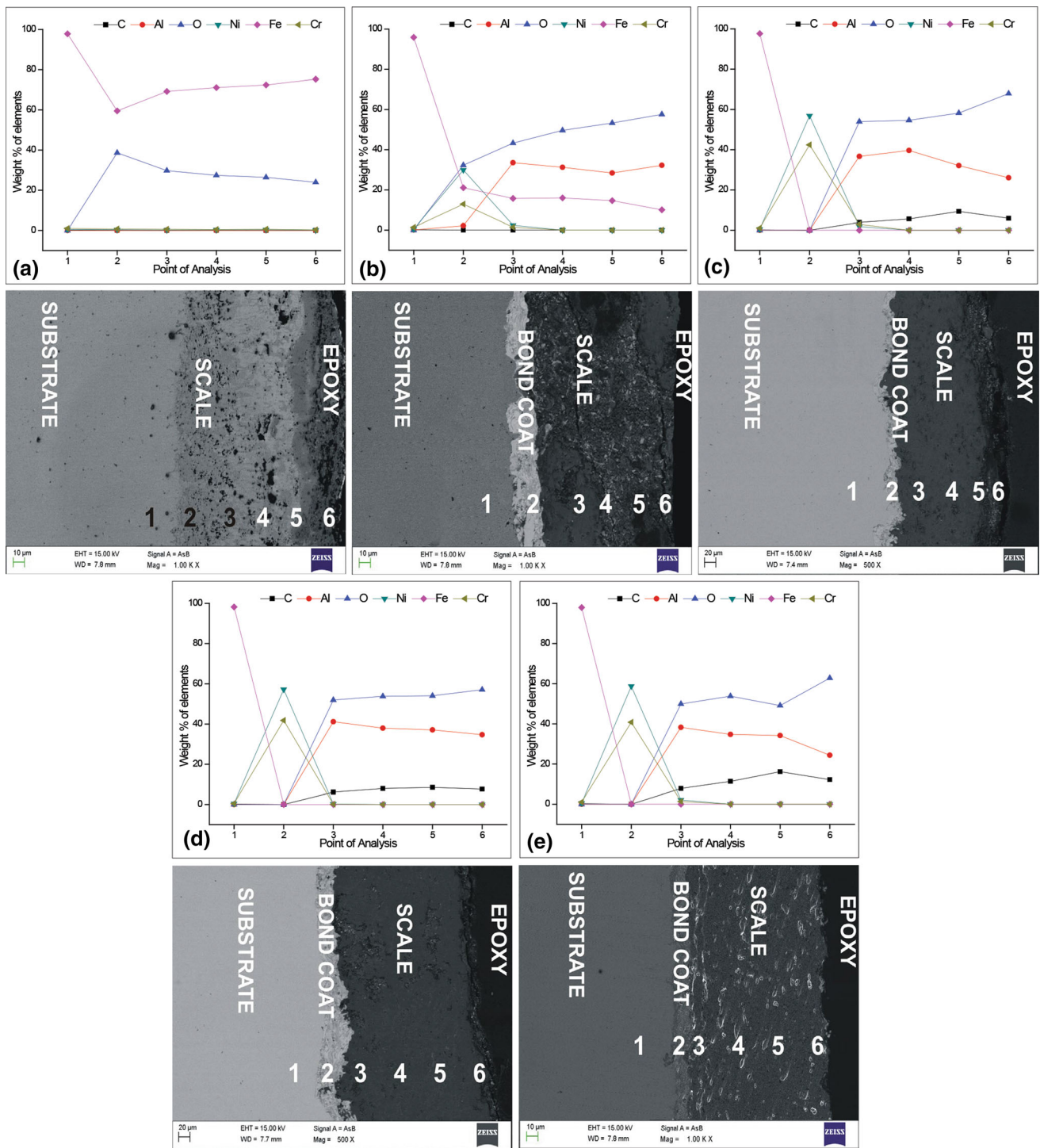


Fig. 8 SEM micrograph and variation in elemental composition across the cross section of (a) bare T11 steel, (b) 0Al₂O₃ coating, (c) 1.5Al₂O₃ coating, (d) 2Al₂O₃ coating, (e) 4Al₂O₃ coating after exposure.

within the scale to form internal sulfides. Therefore, these are the main causes of the corrosion of tube steels in the boilers. Sulfides have not been generally identified in the scale of

samples tested in the boiler (Ref 41). Also, the scale gets removed and regenerated at some locations. It might be because of the erosion, as the coal utilized as a part of Indian power

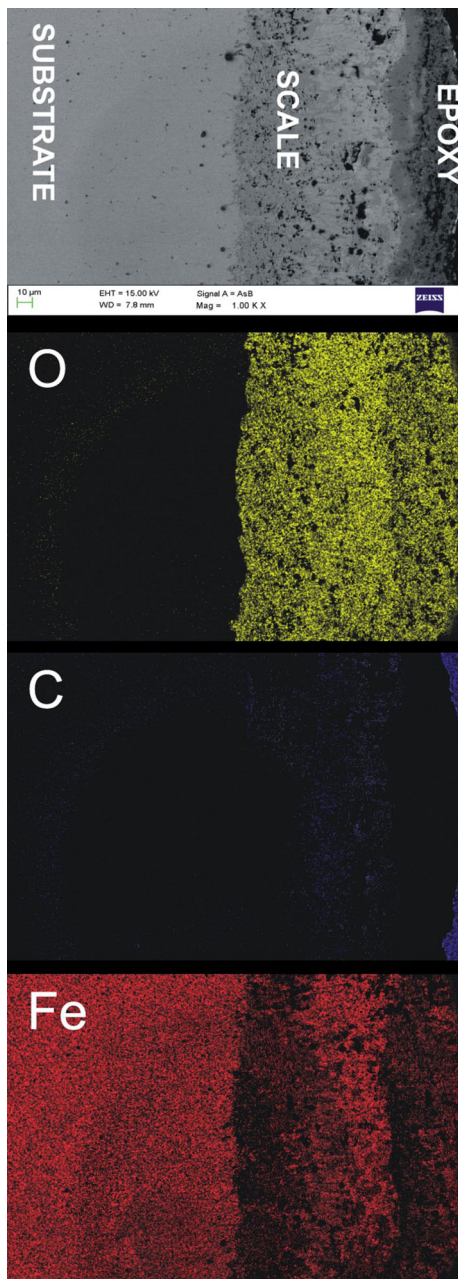


Fig. 9 Composition image and x-ray mappings across the cross section of the T11 steel after exposure.

stations has a lot of slag (around half), which carry rough mineral species, which increment the disintegration inclination of coal.

As the weight change data are not relevant due to the suspected spalling in boiler, the corrosion rate was evaluated in mpy based on the actual thickness of the metal corroded, which is 376.96 mpy in T11 bare steel. As revealed by the XRD diffractograms, Fe_2O_3 and SiO_2 are primary phases in the case of bare steel. The phases revealed by XRD diffractograms are

in agreement with those reported by some authors (Ref 42, 43). Also, development of hematite (Fe_2O_3) as indicated by the XRD has also been revealed by Prakash et al. (Ref 44) and Srikanth et al. (Ref 45). The SiO_2 has been formed because the ash has been deposited on the tubes (Ref 46, 47). The corrosion rate of coated T11 steel is found to be around 47% of the corrosion rate of the bare steel.

XRD diffractograms indicated Al_2O_3 , SiO_2 and Cr_2O_3 phases as reported by Longa-Nova et al. (Ref 42) and Nickel et al. (Ref 43). The formation of Al_2O_3 , Cr_2O_3 and SiO_2 might be because of internal diffusion and ash content deposition (Ref 46). The EDS analysis affirmed the presence of these phases along with confirmation of ash deposition.

The degradation resistance of alumina-coated T11 steel might be because of the dense coating. High corrosion resistance for dense structure has also been reported by Wang (Ref 48). The high resistance of this coating may also be due to nickel chromium band at the interface of bond coat and substrate which might have blocked the movement of degrading elements (Ref 49). The EPMA has confirmed the findings of EDS analysis.

CNT-reinforced Al_2O_3 coating was proven to be very efficient in the coal-fired boiler environment indicating very lesser degradation even after 1000-h exposure at 900 °C. Coating on the samples was intact and no spalling was noticed visually except some deposition of ash. The sequence of corrosion rate in terms of thickness loss for CNT- Al_2O_3 -coated steels followed the sequence:

$$\text{T11} > 0\text{CAI}_2\text{O}_3 > 1.5\text{CAI}_2\text{O}_3 > 2\text{CAI}_2\text{O}_3 > 4\text{CAI}_2\text{O}_3.$$

The maximum resistance to the degradation has been shown by 4CAI₂O₃-coated specimens. This might be attributed to the less porous coating after CNT reinforcement into the alumina matrix. The TEM images for 4CAI₂O₃-coated steel at different magnifications clearly indicated the presence of CNTs in the alumina matrix. The presence of CNTs in alumina matrix might have resulted in a decrease in porosity of alumina coatings. The coating has higher corrosion resistance if it is more compact and of lesser porosity (Ref 48). The nickel- and chromium-rich layer might have been a reason for lower corrosion rate of this coated steel. Comparatively superior corrosion resistance of 4CAI₂O₃-coated T11 might be due to higher percentage of CNTs. XRD graphs indicated the peaks of Al_2O_3 and SiO_2 along with C in the scale. Ahmad et al. (Ref 31) have observed similar peaks during studies on CNT-reinforced alumina composites. SiO_2 may be due to the ash particles present on the surface of specimen. The formation of these compounds has been further validated by EDS as shown in Fig. 7(c), (d) and (e).

CNTs can reduce porosity and improve adhesion between coatings, which is beneficial to decrease the corrosion rate. Apart from that, uniform dispersion and formation of bridges and anchoring between CNTs and Al_2O_3 splats are reasons for blocking the transfer of corrosion species. During the corrosion action, Al_2O_3 may slowly be detached away leaving the carbon nanotubes on the metal surface which impedes the further disintegration of Al_2O_3 matrix and obstructs the transfer of

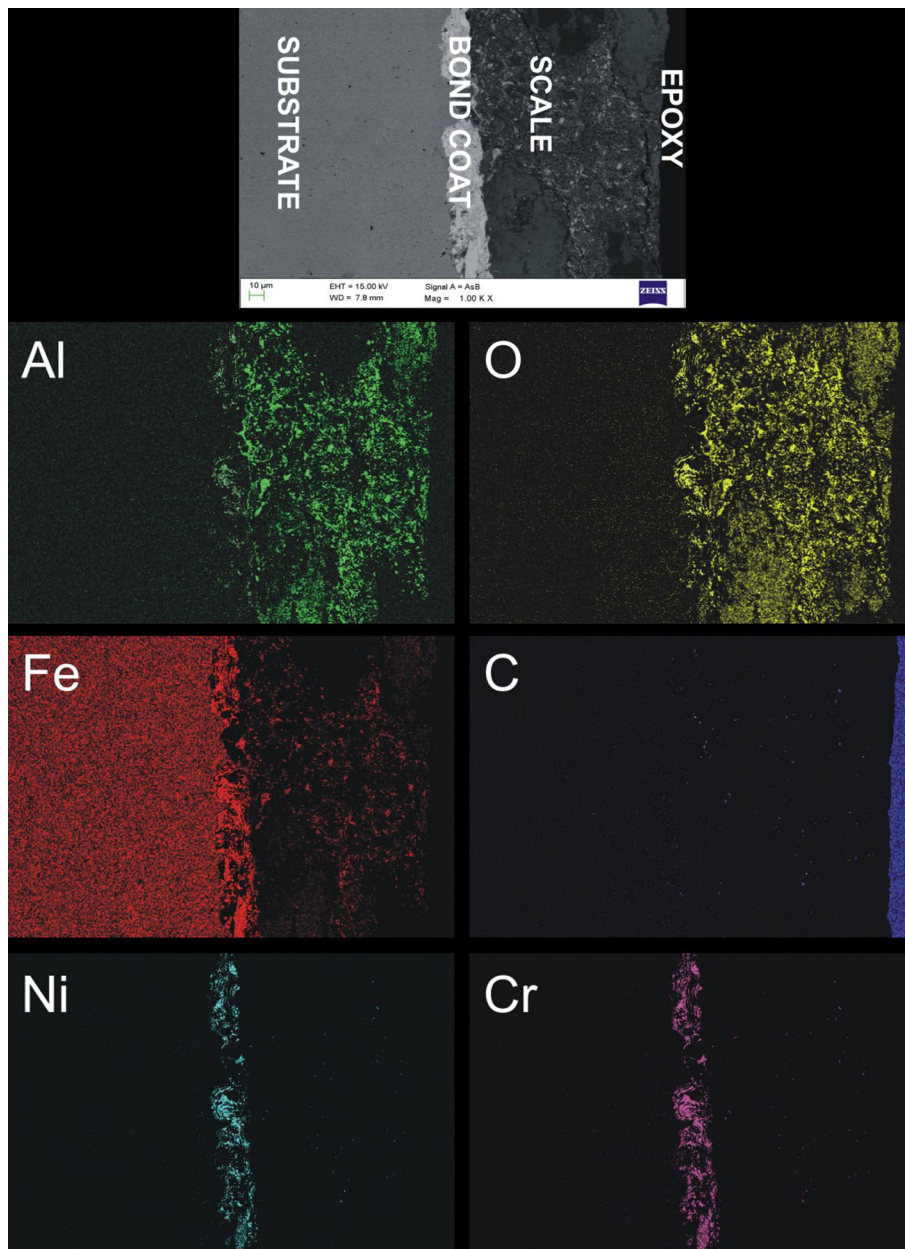


Fig. 10 Composition image and x-ray mappings across the cross section of the plasma-sprayed 0CaAl₂O₃-coated T11 steel after exposure.

corrosive media through it. So, the CNT–Al₂O₃ composite undergoes homogeneous corrosion instead of localized corrosion (Ref 29, 32). The reported results in the present investigation are in close agreement with the findings reported

by Chen et al. (Ref 28) and Praveen et al. (Ref 29) where the authors have reported the high corrosion resistance of CNT-reinforced coatings in corrosive atmospheres.

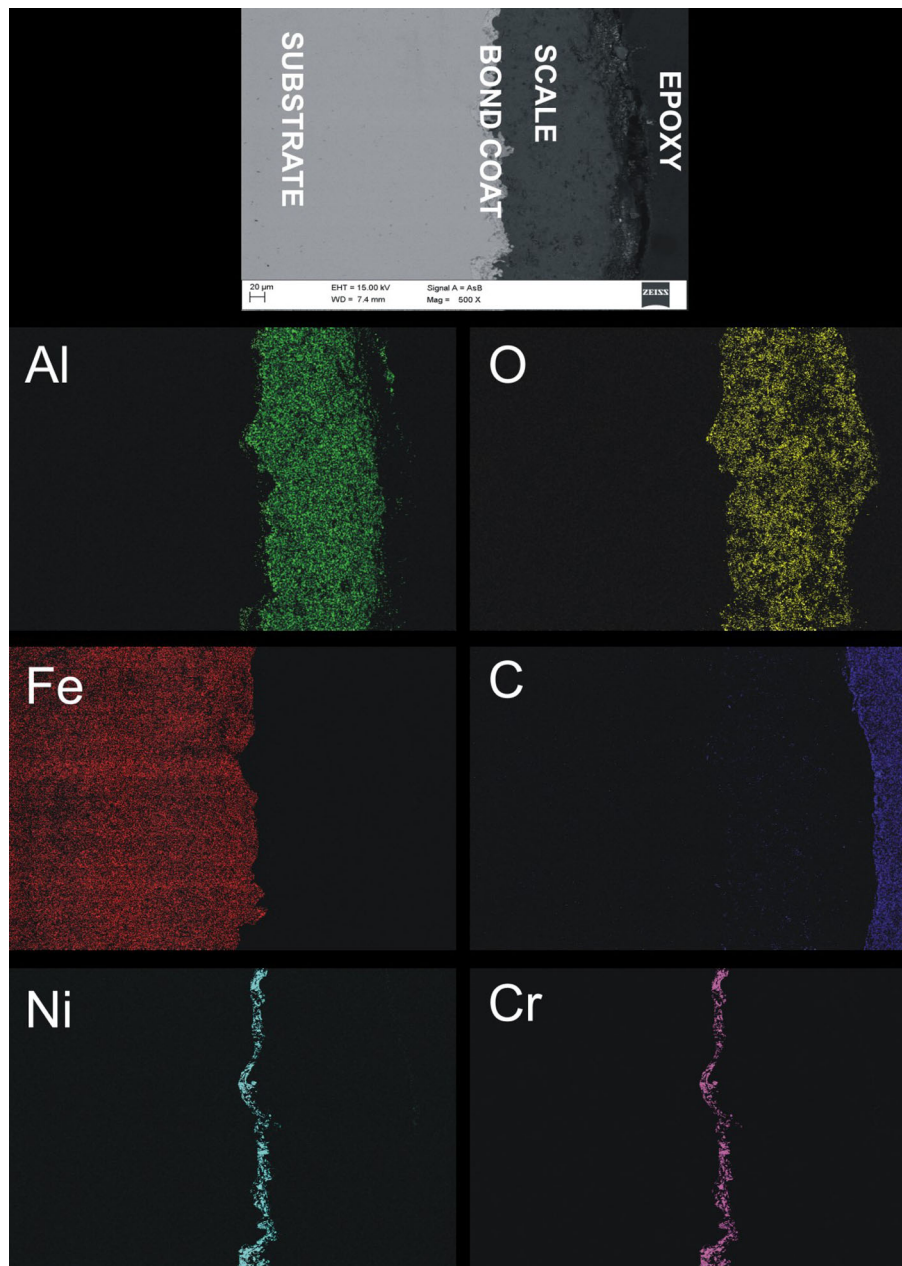


Fig. 11 Composition image and x-ray mappings across the cross section of the plasma-sprayed 1.5CAI₂O₃-coated T11 steel after exposure.

5. Conclusions

The ASME-SA213-T11 boiler steels were coated with Al₂O₃ and CNTs–Al₂O₃ composite coatings and have been exposed to a platen superheater of the coal-fired boiler for 1000 h at 900 °C. The following results are obtained:

1. Uncoated boiler steel has shown severe corrosion. Coatings were proved to be helpful in enhancing the corrosion resistance.
2. Boiler steels coated with Al₂O₃ show better corrosion resistance than uncoated steel.
3. There was a uniform dispersion of CNTs within the alumina coatings.
4. CNT reinforcement has reduced porosity and improved adhesion strength of the alumina coatings.
5. CNT–Al₂O₃ composite undergoes homogeneous corrosion instead of localized corrosion.
6. Coating with a higher percentage of CNTs has higher corrosion resistance. CNTs were easily embedded deeply in the grains of Al₂O₃, filled in cracks and micron-sized holes. These nanotubes behave as blockages to the origination and growth of defect corrosion, improving the microstructure of the alumina layer and therefore improving the resistance to corrosion.

References

1. S. Kamal, R. Jayaganthan, and S. Prakash, Hot Corrosion Studies of Detonation-Gun-Sprayed NiCrAlY + 0.4 wt.% CeO₂ Coated Superalloys in Molten Salt Environment, *J. Mater. Eng. Perform.*, 2011, **20**(6), p 1068–1077
2. T. Sidhu, S. Prakash, and R. Agrawal, Hot Corrosion Resistance of High-Velocity Oxyfuel Sprayed Coatings on a Nickel-Base Superalloy in Molten Salt Environment, *J. Therm. Spray Technol.*, 2006, **15**(3), p 387
3. H. Singh, T. Sidhu, J. Karthikeyan, and S. Kalsi, Evaluation of Characteristics and Behavior of Cold Sprayed Ni-20Cr Coating at Elevated Temperature in Waste Incinerator Plant, *Surf. Coat. Technol.*, 2015, **261**, p 375–384
4. A. López, M. Proy, V. Utrilla, E. Otero, and J. Rams, High-Temperature Corrosion Behavior of Ni-50Cr Coating Deposited by High Velocity Oxygen–Fuel Technique on Low Alloy Ferritic Steel, *Mater. Des.*, 2014, **59**, p 94–102
5. K. Goyal, H. Singh, and R. Bhatia, Current Status of Thermal Spray Coatings for High Temperature Corrosion Resistance of Boiler Steel, *J. Mater. Metall. Eng.*, 2016, **6**(1), p 29–35
6. K. Goyal and R. Goyal, Performance of Cr 3 C 2-25 (Ni-20Cr) and Ni-20Cr Coatings on T91 Boiler Tube Steel in Simulated Boiler Environment at 900°C, *Chem. Mater. Eng.*, 2016, **4**(4), p 57–64
7. X. Zhang, X. Zhang, X. Jie, X. Jie, L. Zhang, L. Zhang et al., Improving the high-temperature oxidation resistance of H13 steel by laser cladding with a WC/Co-Cr alloy coating, *Anti-Corros. Methods Mater.*, 2016, **63**(3), p 171–176
8. V. P. S. Sidhu, K. Goyal, and R. Goyal, Corrosion Behaviour of HVOF Sprayed Coatings on ASME SA213 T22 Boiler Steel in an Actual Boiler Environment. in *Advanced Engineering Forum*, 2017
9. K. Katiki, S. Yadlapati, and S.N.S. Chidepudi, Comparative High Temperature Corrosion Studies on Zirconium Dioxide Coated Inconel 625 in Air and Molten Salt Environment, *Int. J. ChemTech Res.*, 2014, **6**(11), p 4579–45845
10. P. Fauchais, Understanding Plasma Spraying, *J. Phys. D Appl. Phys.*, 2004, **37**(9), p R86
11. B.S. Sidhu, D. Puri, and S. Prakash, Mechanical and Metallurgical Properties of Plasma Sprayed and Laser Remelted Ni-20Cr and Stellite-6 Coatings, *J. Mater. Process. Technol.*, 2005, **159**(3), p 347–355
12. A.N. Khan and J. Lu, Thermal Cyclic Behavior of Air Plasma Sprayed Thermal Barrier Coatings Sprayed on Stainless Steel Substrates, *Surf. Coat. Technol.*, 2007, **201**(8), p 4653–4658
13. L. Du, W. Zhang, W. Liu, and J. Zhang, Preparation and Characterization of Plasma Sprayed Ni 3 Al-hBN Composite Coating, *Surf. Coat. Technol.*, 2010, **205**(7), p 2419–2424
14. K. Goyal, Experimental Investigations of Mechanical Properties and Slurry Erosion Behaviour of High Velocity Oxy Fuel and Plasma Sprayed Cr₂O₃-50% Al₂O₃ Coatings on CA6NM Turbine Steel Under Hydro Accelerated Conditions, *Tribol. Mater. Surf. Interfaces*, 2018, **12**, p 1–10
15. N. Hegazy, M. Shoeib, S. Abdel-Samea, and H. Abdel-Kader, 'Effect of plasma sprayed alumina coating on corrosion resistance'. in *Proceedings of the 13th International Conference on 'Aerospace sciences and aviation technology'*, Cairo, Egypt, 2009, pp. 1–10
16. E. Celik, I. Ozdemir, E. Avci, and Y. Tsunekawa, Corrosion Behaviour of Plasma Sprayed Coatings, *Surf. Coat. Technol.*, 2005, **193**(1), p 297–302
17. N. Malatji, A.P.I. Popoola, O.S.I. Fayomi, and C.A. Loto, Multifaceted Incorporation of Zn-Al₂O₃/Cr₂O₃/SiO₂ Nanocomposite Coatings: Anti-Corrosion, Tribological, and Thermal Stability, *Int. J. Adv. Manuf. Technol.*, 2016, **82**, p 1335–1341
18. S. Deshpande, A. Kulkarni, S. Sampath, and H. Herman, Application of Image Analysis for Characterization of Porosity in Thermal Spray Coatings and Correlation with Small Angle Neutron Scattering, *Surf. Coat. Technol.*, 2004, **187**(1), p 6–16
19. S. Deshpande, S. Sampath, and H. Zhang, Mechanisms of Oxidation and its Role in Microstructural Evolution of Metallic Thermal Spray Coatings—Case study for Ni-Al, *Surf. Coat. Technol.*, 2006, **200**(18), p 5395–5406
20. S. Kamal, R. Jayaganthan, and S. Prakash, Evaluation of Cyclic Hot Corrosion Behaviour of Detonation Gun Sprayed Cr₃C₂-25% NiCr Coatings on Nickel-and Iron-Based Superalloys, *Surf. Coat. Technol.*, 2009, **203**(8), p 1004–1013
21. M.K. Singla, H. Singh, and V. Chawla, Thermal Sprayed CNT Reinforced Nanocomposite Coatings—A Review, *J. Miner. Mater. Charact. Eng.*, 2011, **10**(8), p 717–726
22. B. Yu and M. Meyyappan, Nanotechnology: Role in Emerging Nanoelectronics, *Solid-State Electron.*, 2006, **50**(4), p 536–544
23. K. Liew, X. He, and C. Wong, On the Study of Elastic and Plastic Properties of Multi-Walled Carbon Nanotubes Under Axial Tension Using Molecular Dynamics Simulation, *Acta Mater.*, 2004, **52**(9), p 2521–2527
24. M.-F. Yu, O. Lourie, M.J. Dyer, K. Moloni, T.F. Kelly, and R.S. Ruoff, Strength and Breaking Mechanism of Multiwalled Carbon Nanotubes Under Tensile Load, *Science*, 2000, **287**(5453), p 637–640
25. A. Krishnan, E. Dujardin, T. Ebbesen, P. Yianilos, and M. Treacy, Young's Modulus of Single-Walled Nanotubes, *Phys. Rev. B*, 1998, **58**(20), p 14013
26. A.A. Ali, A. Eldesouky, and S.H. Zoalfakar, Mechanical and Tribological Properties of Hot-Pressed Electrospun MWCNTs/Carbon Nanofibril Composite Fabrics, *Int. J. Adv. Manuf. Technol.*, 2014, **74**(5–8), p 983–993
27. C.I. Park, M. Mostofa, M. Mahmoodi, and S.S. Park, Micromechanical Scribing and Indentation Behavior of Injection-Molded Polymeric Carbon Nanotube (CNT) Nanocomposites, *Int. J. Adv. Manuf. Technol.*, 2013, **68**(1–4), p 391–405
28. X. Chen, C. Chen, H. Xiao, F. Cheng, G. Zhang, and G. Yi, Corrosion Behavior of Carbon Nanotubes–Ni Composite Coating, *Surf. Coat. Technol.*, 2005, **191**(2), p 351–356
29. B. Praveen, T. Venkatesha, Y.A. Naik, and K. Prashantha, Corrosion Studies of Carbon Nanotubes–Zn Composite Coating, *Surf. Coat. Technol.*, 2007, **201**(12), p 5836–5842
30. A.K. Keshri, V. Singh, J. Huang, S. Seal, W. Choi, and A. Agarwal, Intermediate Temperature Tribological Behavior of Carbon Nanotube Reinforced Plasma Sprayed Aluminum Oxide Coating, *Surf. Coat. Technol.*, 2010, **204**(11), p 1847–1855
31. I. Ahmad, M. Unwin, H. Cao, H. Chen, H. Zhao, A. Kennedy et al., Multi-walled Carbon Nanotubes Reinforced Al₂O₃ Nanocomposites: Mechanical Properties and Interfacial Investigations, *Compos. Sci. Technol.*, 2010, **70**(8), p 1199–1206
32. K. Balani, S.P. Harimkar, A. Keshri, Y. Chen, N.B. Dahotre, and A. Agarwal, Multiscale Wear of Plasma-Sprayed Carbon-Nanotube-Reinforced Aluminum Oxide Nanocomposite Coating, *Acta Mater.*, 2008, **56**(20), p 5984–5994
33. C.F. Gutierrez-Gonzalez, A. Smirnov, A. Centeno, A. Fernández, B. Alonso, V.G. Rocha et al., Wear Behavior of Graphene/Alumina Composite, *Ceram. Int.*, 2015, **41**(6), p 7434–7438
34. W. Guo and H.-Y. Tam, Effects of Carbon Nanotubes on Wear of WC/Co Micropunches, *Int. J. Adv. Manuf. Technol.*, 2014, **72**(1–4), p 269–275
35. R. Goyal, B.S. Sidhu, and V. Chawla, Characterization of Plasma-Sprayed Carbon Nanotube (CNT) -Reinforced Alumina Coatings on ASME-SA213-T11 Boiler Tube Steel, *Int. J. Adv. Manuf. Technol.*, 2017, **92**, p 3225–3235
36. K. Weulersse-Mouturat, G. Moulin, P. Billard, and G. Pierotti, VII Land-Based Gas Turbines, Diesel Engines, Boilers, Incinerators, Burners, Coal Gasification, Aerospace Industry-High Temperature Corrosion of Superheater Tubes in Waste Incinerators and. in *Materials Science Forum*, 2004, pp. 973–980
37. T. Sidhu, S. Prakash, and R. Agrawal, Studies of the Metallurgical and Mechanical Properties of High Velocity Oxy-Fuel Sprayed Stellite-6 Coatings on Ni- and Fe-Based Superalloys, *Surf. Coat. Technol.*, 2006, **201**(1), p 273–281
38. T. Sidhu, S. Prakash, and R. Agrawal, Hot Corrosion Studies of HVOF Sprayed Cr₃C₂-NiCr and Ni-20Cr Coatings on Nickel-Based Superalloy at 900 °C, *Surf. Coat. Technol.*, 2006, **201**(3), p 792–800
39. K. Weulersse, G. Moulin, P. Billard, and G. Pierotti, High Temperature Corrosion of Superheater Tubes in Waste Incinerators and Coal-Fired Plants. in *Materials Science Forum*, 2004, pp. 973–980
40. S. Srivastava, K. Godiwalla, and M. Banerjee, Fuel Ash Corrosion of Boiler and Superheater Tubes, *J. Mater. Sci.*, 1997, **32**(4), p 835–849
41. H. Crossley, A. Poll, and F. Sweett, The Reduction of Sulphur Trioxide by Constituents of Boiler Flue Dust, *J. Inst. Fuel*, 1948, **21**, p 207–209
42. Y. Longa-Nava, Y. Zhang, M. Takemoto, and R. Rapp, Hot Corrosion of Nickel–Chromium and Nickel–Chromium–Aluminum Thermal-Spray Coatings by Sodium Sulfate–Sodium Metavanadate Salt, *Corrosion*, 1996, **52**(9), p 680–689

43. H. Nickel, W. Quadackers, and L. Singheiser, Analysis of Corrosion Layers on Protective Coatings and High Temperature Materials in Simulated Service Environments of Modern Power Plants using SNMS, SIMS, SEM, TEM, RBS and X-ray Diffraction Studies, *Anal. Bioanal. Chem.*, 2002, **374**(4), p 581–587
44. S. Prakash, S. Singh, B. Sidhu, and A. Madeshia, Tube Failures in Coal Fired Boilers. in *Proceedings of the National Seminar on Advances in Material and Processing*, 2001, pp. 9–10
45. S. Srikanth, B. Ravikumar, S.K. Das, K. Gopalakrishna, K. Nandakumar, and P. Vijayan, Analysis of Failures in Boiler Tubes due to Fireside Corrosion in a Waste Heat Recovery Boiler, *Eng. Fail. Anal.*, 2003, **10**(1), p 59–66
46. R. John, Slag, Gas, and Deposit Thermochemistry in a Coal Gasifier, *J. Electrochem. Soc.*, 1986, **133**(1), p 205–211
47. B. M. Institute, A. R. C. o. Corrosion, and D. f. C. Gases, A Review of Available Information on Corrosion and Deposits in Coal and Oil-fired Boilers and Gas Turbines: Report of ASME Research Committee on Corrosion and Deposits from Combustion Gases. *American Society of Mechanical Engineers*, 1959
48. B. Wang, Erosion-Corrosion of Thermal Sprayed Coatings in FBC Boilers, *Wear*, 1996, **199**(1), p 24–32
49. B.S. Sidhu and S. Prakash, Evaluation of the Corrosion Behaviour of Plasma-Sprayed Ni₃Al Coatings on Steel in Oxidation and Molten Salt Environments at 900 °C, *Surf. Coat. Technol.*, 2003, **166**(1), p 89–100
50. S.R. Kiahosseini and A. Aminian, Mechanical and Corrosion Performance of Multilayer Ceramic Coatings Deposited on an Austenitic Stainless Steel Using Plasma Spray, *Bull. Mater. Sci.*, 2019, **42**(160), p 1–7
51. A.K. Shirazi and S.R. Kiahosseini, Hot Corrosion of the Ceramic Composite Coating Ni₃Al-Al₂O₃-Al₂O₃/MgO Plasma Sprayed on 316L Stainless Steel, *Int. J. Mater. Res.*, 2017, **108**(8), p 675–680
52. A. Mangla, V. Chawla, and G. Singh, Comparative Hot Corrosion Behavior of HVOF and Plasma Sprayed Ni₂₀Cr Coated T-22 Steel in Actual Coal Fired Boiler Environment, *Global J. Eng. Sci. Res.*, 2017, **4**(11), p 6–19
53. R. Goyal, B. Sidhu, and V. Chawla, Improving the High-Temperature Oxidation Resistance of ASME-SA213-T11 Boiler Tube Steel by Plasma Spraying with CNT-Reinforced Alumina Coatings, *Anti-Corros. Methods Mater.*, 2018, **65**(2), p 217–223
54. G. Yang, C. Li, C. Li, K. Kondoh, and A. Ohmori, Improvement of Adhesion and Cohesion in Plasma-Sprayed Ceramic Coatings by Heterogeneous Modification of Nonbonded Lamellar Interface Using High Strength Adhesive Infiltration, *J. Therm. Spray Technol.*, 2013, **22**, p 36–47

Publisher's Note Springer Nature remains neutral with regard to jurisdictional claims in published maps and institutional affiliations.